Effects of forming parameters on the forming limit of single-point incremental forming of sheet metal

Chunjian Su[1] · Shipeng Lv[1] · Rui Wang[1] · Yuting Lv[1] · Shumei Lou[1] · Qing Wang[2] · Sumin Guo[1]

Abstract

In this paper, experimental and numerical simulation studies on the forming limit diagram of single-point incremental forming (SPIF) were described. We proposed a novel method for evaluating the forming limit in incremental forming. The proposed method utilizes the forming limit angle and the maximum thinning rate. The effects of the forming and processing parameters on the forming limit of an aluminum sheet during incremental forming were investigated using a combination of simulation analysis and experimental verification. The obtained results show that the forming limit is large for 1060Al and 6061Al when the initial thickness is 1.5 mm for a single parameter change for SPIF. For 1060Al, the step size is in the range of 0.8–1.5 mm. When the step size is 0.8 mm, the incremental forming limit is large and the forming precision is high. For 1060Al and 6061Al, the incremental forming limit is at the maximum level when the tool radius is 6.0 mm, and when the tool radius is 5.0 mm, the best forming precision can be achieved. It is of great theoretical significance and practical engineering value to study the effects of various forming parameters on the forming limit of metal sheet SPIF.

1 Introduction

The sheet metal single-point incremental forming (SPIF) technology is one of the flexible manufacturing technologies in which the sheet is locally deformed successively instead of integral forming, and finally the sheet is formed into the required workpiece. Many studies showed that SPIF, compared with traditional stamping technology, could effectively control the metal flow of the sheet, increase the forming limit of the sheet, and reduce the forming force during the forming process. There is growing interest on SPIF research due to its substantial importance in improving and developing of sheet metal forming theory. It also provides more opportunities for the designing of new products.

SPIF is based on the relative movement of a simple small punch concerning the sheet. The main advantages of SPIF include high flexibility as well as no requirement for a die to obtain the final shape of components as reported by Gu et al. [1]. The SPIF technology has been frequently studied, applied, and perfected for metal sheet manufacturing, especially titanium and its alloys in some industrial sectors such as aerospace, chemical engineering, and medical surgery according to Nguyen et al. [2]. The incremental sheet forming process is a rapid prototyping technology that fulfills the current requirements for flexible, sustainable, and economical manufacturing technologies viable for small and medium-sized batches, without necessarily using expensive dedicated machines or equipment. These characteristics make this process very suitable for the manufacturing of customized parts from metal or polymeric sheets, according to Centeno et al. [3].

Many scholars have conducted extensive research on the processing parameters and forming limits of the SPIF. McAnulty et al. [4] reviewed the literature on sheet metals using the process parameters such as material thickness, tool shape, spindle speed, tool diameter, feed rate, and tool rotation, which improve the formability. Uheida et al. [5] conducted an experimental study to investigate the effects of tool rotation direction during the SPIF of pure titanium. Raju

✉ Sumin Guo
  sdkjjd314@163.com

  Shipeng Lv
  lvshipeng2018@163.com

[1] College of Mechanical and Electronic Engineering, Shandong University of Science and Technology, Qingdao 266590, China

[2] School of Civil Engineering and Architecture, Shandong University of Science and Technology, Qingdao 266590, China

et al. [6] examined the possibility of using low thickness multiple sheets in a SPIF process; their results showed the mechanism of sheet failure, new surface generation, and the extent of achievable forming limits from the top sheet to the bottom sheet while forming multiple sheets together. Eyckens et al. [7] used the MK-type analysis to show the effect of through-thickness shear on the forming limit curve (FLC). They demonstrated that shear could raise the FLC significantly, but this phenomenon depends on the orientation of the shear. Buffa et al. [8] proposed a new approach to enhance the material formability through a localized sheet heating as a consequence of the friction work caused by elevated tool rotational speeds. In addition, they observed a significant increase in the material formability for three materials (AA1050-O, AA1050-H24, and AA6082-T6 were utilized), and new formability curves have been built by the varying the utilized rotational speed. Ramkumar et al. [9] assessed the formability of the sheet metal along with the surface roughness using the forming limit diagram (FLD) and void analysis. The roughness value of the sheet metals formed was analyzed using the three-dimensional (3D) surface roughness tester. The obtained results showed higher formability and better surface finish could be achieved by multipoint forming tool compared to the single-point forming tool.

Numerical simulation is essential for SPIF to predict the fracture and forming limit during the forming process. The instantaneous stress state variables and the evolution of the nonlinear strain path can be obtained. Numerical simulation and experiment can jointly verify the accuracy of the results. Mirnia et al. [10] investigated the ductile fracture in SPIF by implementing the phenomenological modified Mohr-Coulomb (MMC3) model through an appropriate user subroutine using the commercial FE code Abaqus/Explicit. The comparison of predicted and experimental fracture depths of SPIF parts demonstrated that utilizing the MMC3 criterion has 10% discrepancy on average. Good agreement of the fracture location can also be found between experiments and FE simulations. Numerically computed fracture strains showed that the fracture forming limit diagram (FFLD) under a proportional loading, like a tensile test, differed in shape and value from the one obtained under a non-proportional loading like SPIF in which the FFLD is higher. Zhan et al. [11] calibrated the flow stress model and thermal ductile fracture criterion and integrated with the numerical simulation of SPIF process for AA2024-T3 under high-speed tool rotation, and a novel numerical-analytical model is proposed to calculate the damage accumulation. Zhang et al. [12] presented a novel flexible forming process called incremental bending. They investigated the formability of this process based on experiments and a numerical simulation. Esmaeilpour et al. [13] used the Yld2004-18p as a non-quadratic anisotropic 3D yield function for the finite element simulation of incremental forming processes. For this purpose, a VUMAT was developed to employ

this yield function in ABAQUS. Considering that von Mises and Hill's 1948 yield functions are special cases of the 3D Yld2004-18p yield function, the same VUMAT was used to simulate SPIF for a conical geometry using the three yield functions. Thus far, no uniform evaluation method has been proposed for studying forming limits in incremental forming.

This paper proposes a FLD by combining the forming limit angle and the maximum thinning rate. We applied FLD to evaluate the forming limit in incremental forming. We used a simulation analysis and experimental verification to investigate the effects of forming and processing parameters on the forming limit of aluminum sheets during incremental forming. The FLD can help to optimize sheet forming properties and improve forming quality.

2 Theoretical forming limit for numerically controlled SPIF

In this paper, we mainly analyze the forming limit angle and the thinning rate for SPIF.

As shown in Fig. 1, θ is the forming angle and α is the half-cone angle. The two angles are complementary to each other. When θ is the limit angle, the minimum value is called the limit half-cone angle reported by Esmaeilpour et al. [13].

According to the principle of constant volume (Eq. (1)) claimed by Silva et al. [14]:

$$t = t_0 \sin(90° - \theta) \tag{1}$$

where t_0 is the thickness of the sheet before forming in millimeters and t is the thickness of the sheet after forming in millimeters.

According to the above sinusoidal function relationship, when θ is close to 90°, the thickness t of the deformed sheet is close to 0. Cracking occurs when the thickness of the sheet is reduced too much according to Cho et al. [15]. Therefore,
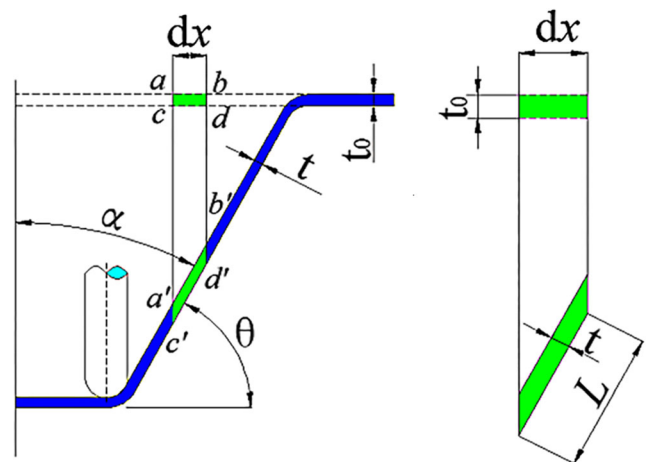

Fig. 1 Single-point incremental forming sheet deformation

we can prevent cracking of the sheet by controlling the forming angle.

The average thinning rate is the percentage difference in the wall thickness before and after forming showed in Eq. (2) reported by Nichols et al. [16]:

$$\Psi_t = \frac{t_0 - t}{t_0} \times 100\% \qquad (2)$$

The logarithmic thinning rate (Eq. (3)) is the logarithmic rate of change of thickness according to Lee et al. [17]:

$$\eta_t = ln\frac{t_0}{t} \times 100\% \qquad (3)$$

Combining the above, we obtain Eq. (4) and Eq. (5):

$$\Psi_t = (1 - \sin\alpha) \times 100\% \qquad (4)$$

$$\eta_t = ln\frac{1}{\sin\alpha} \times 100\% = -(ln\sin\alpha) \times 100\% \qquad (5)$$

Using the above formula, the relationship between the half-cone angle and the thinning rate is shown in Fig. 2. It can be seen from the figure that the average thinning rate and the logarithmic thinning rate decrease with the forming half-cone angle, but at a different rate. In actual SPIF, once the sheet breaks, the entire forming process has failed. Thus, the final failure of the sheet depends on the maximum thinning rate, not the average thinning rate.

In summary, the variation of the wall thickness of an incrementally formed part depends on the sine of the half-cone angle. The maximum thinning rate of the sheet reflects the maximum forming limit. If this theory for the variation in wall thickness in incremental forming can be confirmed for some less complex shaped parts, it is possible the forming limit half-cone angle and the maximum thinning rate can be combined into a predictive metric for sheet forming.
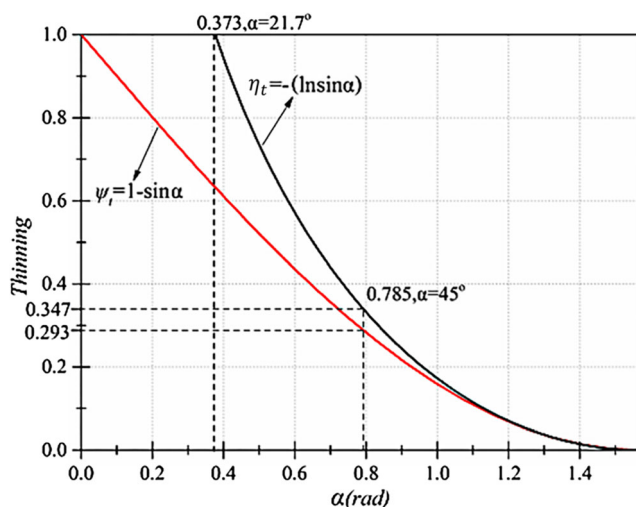

Fig. 2 Relationship between the half-cone angle and the attenuation rate

3 Simulations and experiments

3.1 Finite element simulations

The simulation part is a cone. Its size and shape are shown in Fig. 3. For the simulation board, we used sheets of 1060Al and 6061Al. Table 1 lists the chemical composition and other parameters of the simulated materials reported by Kim et al. [18]. Tungsten steel was selected for the forming tool head. The finite element model was built using 3D software and meshed (grid size 1 mm). The finite element model after meshing is shown in Fig. 4. In this simulation, limiting the unique degree of freedom around the sheet is used instead of the fixing effect of the binder ring on the sheet. Table 2 shows the diameter of the forming tool head, axial feed amount, and initial sheet thickness for each test. The tool rotational speed was 3000 r/min and the feed rate was 300 mm/min. The spiral path of tool head is shown in Fig. 5. The solver ANSYS/LS-DYNA was used for the simulation.

3.2 Experiment

3.2.1 Electrochemical etching

Electrochemical etching was used to create a grid pattern on the blank metal test sheet before being deformed by machining. In the experiment, the pattern was a dense circular grid (3 mm diameter). The template was carefully placed on the surface of the sheet. A felt pad was placed on top of the template and the electrode wheel pressed the felt pad against the template. The power supply was connected to the electrode and sheet blank claimed by Cho et al. [15]. The roller electrode connected to the power source reciprocated on the felt pad, so current was transferred from the electrode to the blank. The roller formed a profile on the sheet. After etching, the metal piece was washed with a neutralizing solution. This produced a grid of circles, as shown in Fig. 6.

3.2.2 SPIF experiment

In this experiment, we used a platform based on a VC850 NC machining center. The hemispherical forming tool head used in the experiment was made of YG8 tungsten steel. The plates used in the experiment were made of 1060Al and 6061Al. Each sheet was a square with a side length of 300 mm. As shown in Fig. 7(a), the experimental platform, which includes the fixing device, the supporting device, and the splint, was placed on the processing platform of the NC machining center. We loaded a pre-written program into the NC machining center and then we moved the tool head to the center of the machined sheet. The forming tool head followed the pre-programmed trajectory while the NC machining center

Fig. 3 Conical simulation part
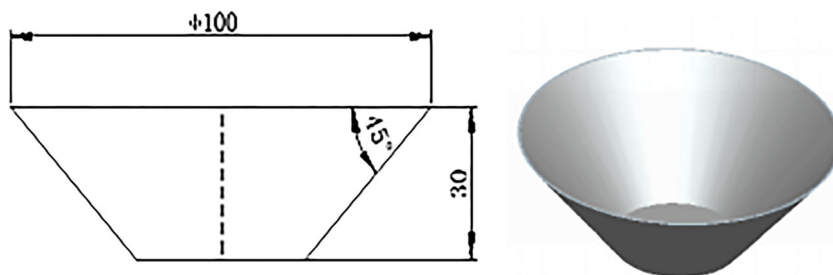
Table 1 Composition and properties of 1060Al and 6061Al

Material	Chemical composition (%)								
	Al	Si	Cu	Mg	Zn	Mn	Ti	V	Fe
1060Al	99.6	0.25	0.05	0.03	0.05	0.03	0.03	0.05	0.05
6061Al	96.1	0.6	0.25	1.02	0.25	0.15	0.15		0.7
Material	Performance parameter								
	Density (kg/m^3)		Tensile strength (MPa)			Yield strength (MPa)			
1060Al	2680		95.32			42.58			
6061Al	3130		124.23			55.67			

supplied lubricant (Grade-68 Hydraulic oil) through a nozzle. Figure 7(b) shows a machined part.

We ran seven sets of experiments for each of the two materials. The experimental parameters are shown in Table 2. For each set of experiments, we ran the test four times and the average was taken. The median method was used to find the maximum forming limit angle for each set of plates. Measure the thickness of the deformed sheet with an accuracy of 0.001 mm micrometer to obtain the thinning rate. An experimental forming limit diagram was drawn using the strain measurement grid method. The transverse and longitudinal deformations of the experimental fracture diagram grid were
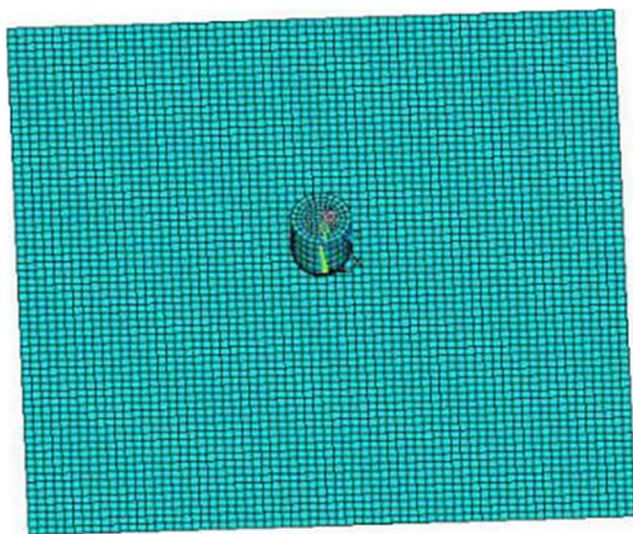

Fig. 4 Finite element model of grid

measured by GMA System, and the primary strain and secondary strain were obtained. The forming limit was obtained using numerical fitting.

4 Results and discussion

4.1 Effect of initial plate thickness on forming limit of SPIF sheet

4.1.1 Effect of initial thickness on forming limit angle

For tests 1, 5, and 6, we formed parts through SPIF from sheets made of 1060Al and 6061Al. Figure 8(a) shows the thickness of a simulated sheet and Fig. 8(b) shows the measurement positions of an experimental sheet. We used the median method to find the maximum forming limit angle of each plate, as shown in Table 3.

The relationship between the sheet thickness and the forming limit angle is shown in Fig. 9. As can be seen, the forming limit angle of the sheet increases as the initial thickness of the sheet increases.

From the data in Table 3, we can see that the theoretical logarithmic thinning rates of 1060Al and 6061Al, for a thickness of 1.5 mm, are 100.30% and 100.80%, respectively, which is unreasonable. The logarithmic thinning rate and the average thinning rate are quite different from the measured thinning rates. Therefore, we conclude that Eqs. (2–4) and (2–5) do not accurately reflect the thinning rate of a sheet when it is incrementally formed to the forming limit angle.

Table 2 Experimental settings

Number	Initial plate thickness (mm)	Step size (mm)	Tool radius (mm)
1	1	1	5
2	1	1.5	5
3	1	1	4
4	1	1	6
5	0.8	1	5
6	1.5	1	5
7	1	0.8	5

The simulated maximum thinning rate and the experimental maximum thinning rate are not too different. Hence, the simulated maximum thinning rate can be used as a proxy for the experimental maximum thinning rate. Therefore, the forming angle and the maximum thinning rate can be used to determine the forming limit of a sheet during incremental forming into a simple shape.

Figure 10 shows forming limit curves. To the left of the ordinate is the angle area. The angle of the line is the forming angle of the workpiece. To the right of the ordinate is the thinning rate area. The height of the line represents the reduction ratio. The forming limit curves for sheets of 1060Al and 6061Al with the same thickness are different. This method can be used to determine quickly and easily the maximum forming limit of sheets of 1060Al and 6061Al for different thicknesses. However, this method does not apply to the forming limit for asymmetrical or complex forming, or for a variable forming angle.

4.1.2 Effect of initial thickness on the forming limit diagram

Table 4 compares ruptures from the experiments and the simulations for sheets of 1060Al and 6061Al with an initial
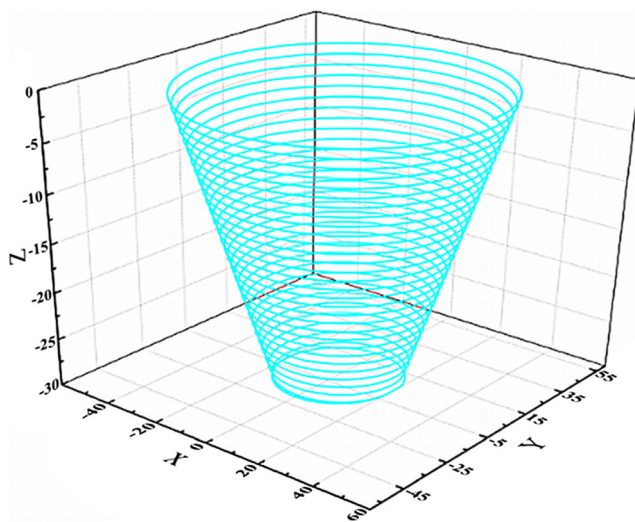
thickness of 1.0 mm machined by SPIF. It can be seen that the ruptures of the plate in the simulation are roughly consistent with the ruptures in the experiments. Thus, the simulation can approximate what happens to a plate during SPIF.

Figure 11 shows simulated forming limit diagrams of 1060Al and 6061Al after SPIF for an initial plate thickness of 1.0 mm. Figure 12 shows experimental forming limit diagrams for 1060Al and 6061Al for different initial plate thicknesses.

A forming limit curve divides the primary and secondary strain scatter plot into two areas, a safe zone and a non-safe zone. The non-safe area is above the straight line, in which a plate may break when it is gradually formed by SPIF. Below the line is the safe area, where a part can be formed stably. Therefore, the maximum forming performance of a sheet during incremental forming can be evaluated intuitively.

As can be seen from Fig. 12, the forming limit of a sheet during SPIF is approximately a straight line with a slope of −1. The forming limit depends on the initial sheet thickness. We compared sheets made from the same material but with


Fig. 5 Spiral path of tool head
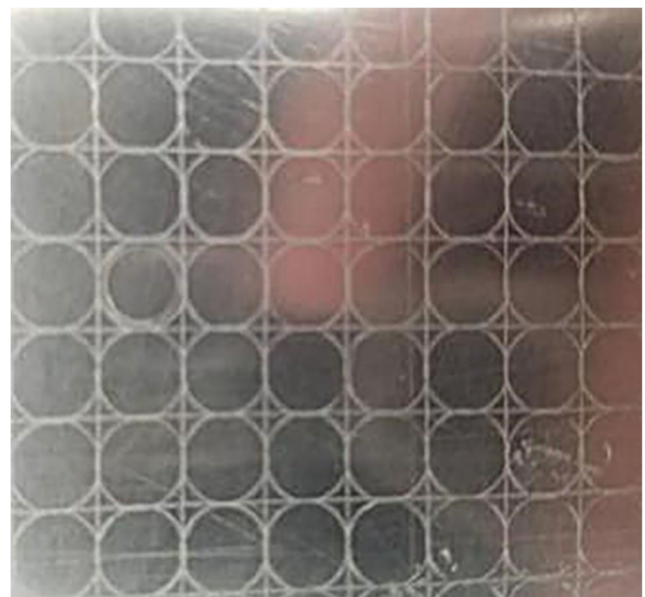
Fig. 6 Pattern formed on metal sheet

Fig. 7 Equipment: (**a**) experimental platform, (**b**) formed part
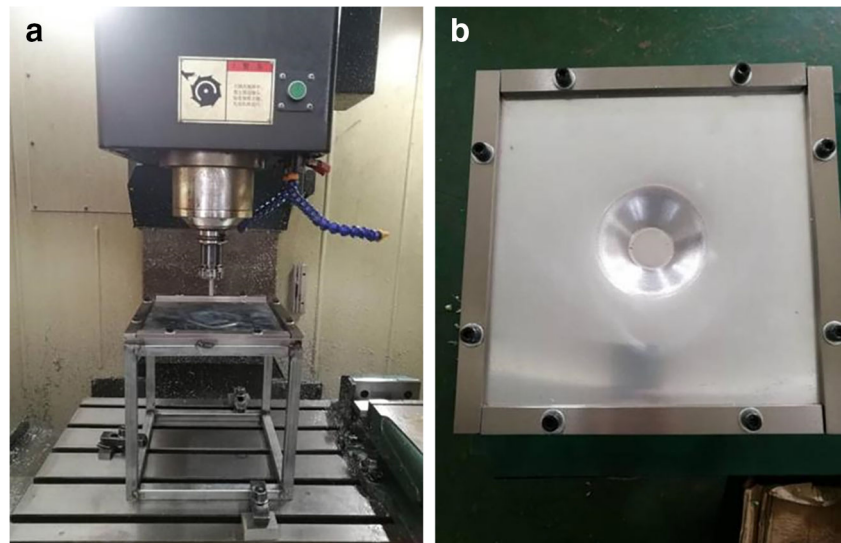
different initial thicknesses in Fig. 13. The results show that the larger the initial plate thickness, the higher the forming limit.

To obtain the forming limit curve of a sheet during incremental forming, we select the highest points (red scatter) in
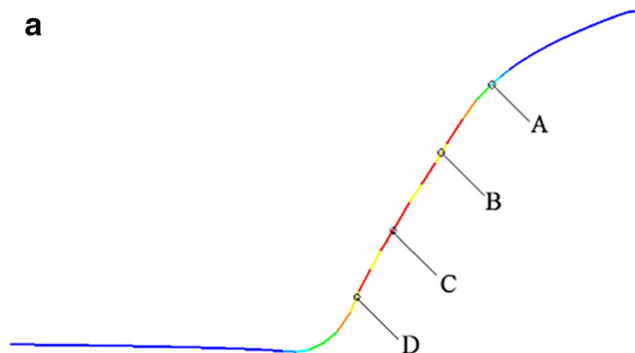
Fig. 8 Sheets thickness: (**a**) simulation, (**b**) experimental

Fig. 11. In Fig. 14, we compare the numerical fitting lines with the experimental fitting lines. It can be seen from this figure that the fit to the forming limit from the simulation and the one from the experiment are very similar. The forming limit diagram obtained from a simulation can effectively predict the forming limit of a sheet during SPIF.

In summary, we have produced forming limit diagrams of the two materials for different initial thicknesses using simulation and experiments. We conclude that in incremental forming, the forming limit depends on the initial thickness, within a certain thickness range. The thicker the initial plate, the higher the forming limit.

## 4.2 Effect of step size on forming limit of SPIF sheet

4.2.1 Effect of step size on forming limit angle

The tool head moves spirally around the inside of the part with a rotation speed of 3000 r/min and a feed speed of 300 mm/min. Each turn machines a layer of the part. After one complete turn, it has moved vertically down by a distance known as the step size. The step size affects both the forming limit angle of the sheet and the forming precision. If the step size is too large, the sheet may not be formed and the forming equipment may be damaged. A small step size will reduce production efficiency and increase production cycle times. Thus, the best step size is moderate.

To use the forming angle and the maximum thinning rate to describe the forming limit of a sheet during incremental forming, it is necessary to consider the simulation and the experiment to measure the thinning rate of the formed sheet at the forming limit angle. The forming limit angles and maximum thinning rates of 1060Al and 6060Al sheets of different step sizes are shown in Table 5. Other parameters are shown in Table 2. As the step size increases, the limit angle of sheet

Table 3 Summary of results for 1, 5, and 6 tests

Material	Thickness (mm)	Forming limit angle (°)	Thinning rate			
			Logarithmic thinning rate	Average thinning rate	Maximum thinning rate	
					Simulation	Experiment
1060Al	0.8	66.4	91.94%	60.13%	78.25%	82.62%
	1	67.2	94.80%	61.25%	79.38%	84.28%
	1.5	69.2	100.30%	64.49%	82.81%	87.32%
6061Al	0.8	65.2	86.88%	58.05%	76.12%	79.86%
	1	66.8	93.16%	60.61%	78.57%	81.58%
	1.5	68.6	100.80%	63.51%	79.61%	83.36%
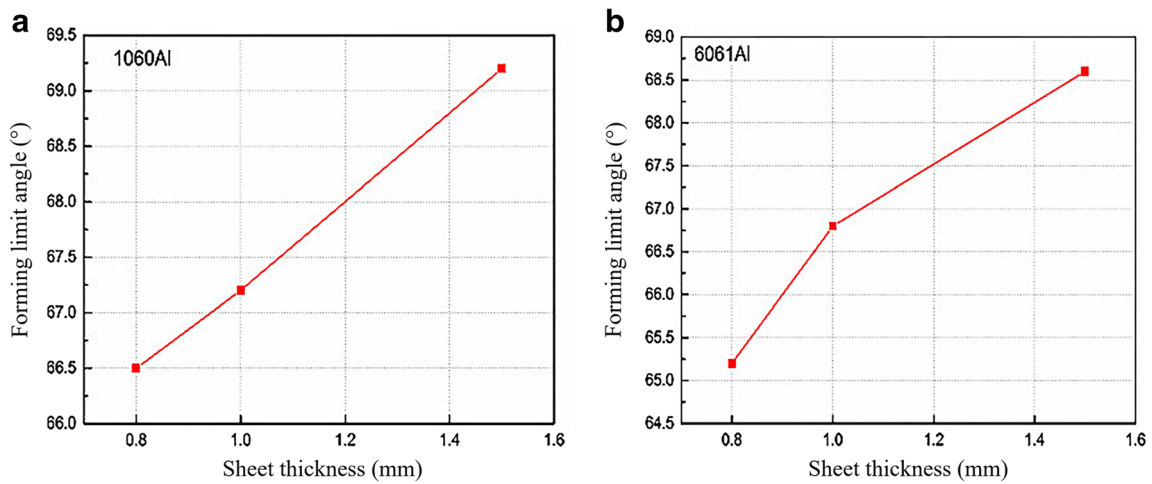
Fig. 9 Relationship between initial thickness and forming limit angle: (**a**) 1060Al, (**b**) 6061Al
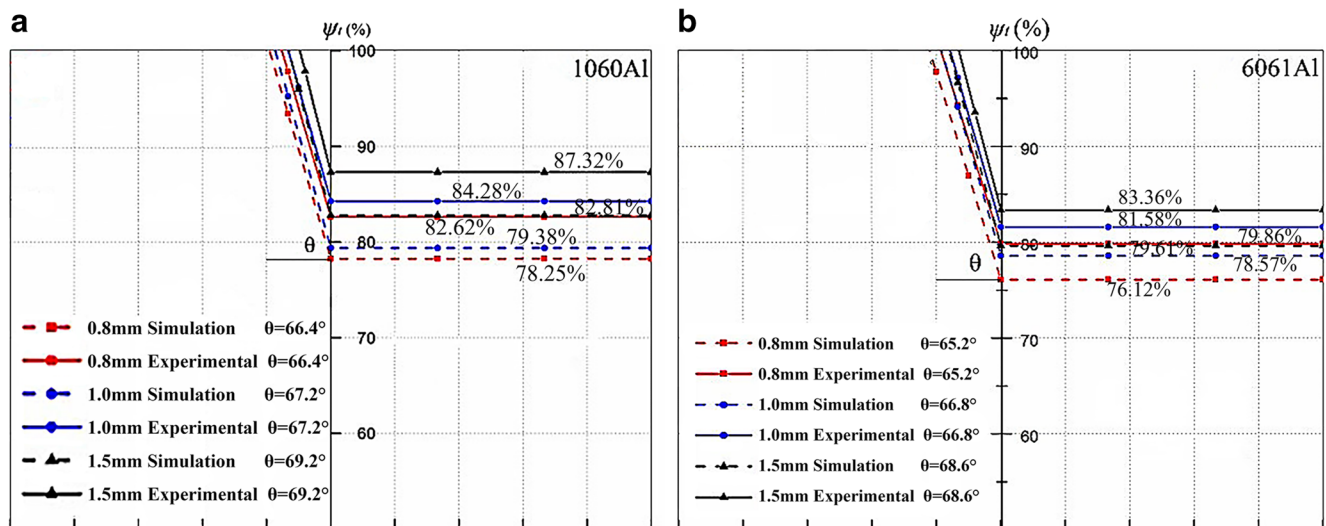
Fig. 10 Angle and thinning rate forming limit curves: (**a**) 1060Al, (**b**) 6061Al

Table 4 Comparison of ruptures from the experiments and the simulations
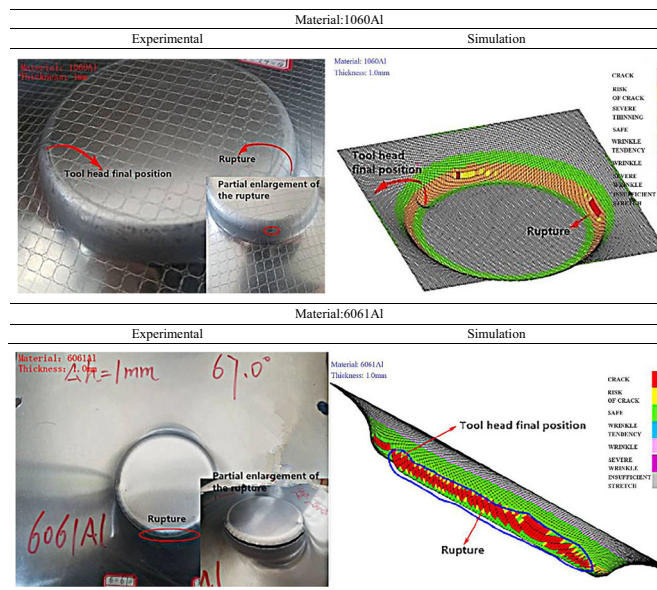
metal forming decreases. This relationship is shown in Fig. 15.

Figure 16 shows the parts machined from 1060Al with an initial thickness of 1 mm, a tool radius of 5 mm, the same lubrication conditions, and a step size of 0.8, 1.0, or 1.5 mm. It can be seen from the figure that when the step size is 1.5 mm, the starting edge has severe edging. The texture at the middle of the part is rough. Overall, the forming quality is poor. When the step size is 0.8 mm, the starting edge of the formed part has slight edging and the texture in the middle is clearly better. The finish is good. The forming quality is much better than when the step size is 1.5 mm. The back side of the formed part is also much smoother than when the step size is 1.5 mm, where there is significant layer-by-layer processing trace.

As can be seen from Fig. 17, the forming angle and the maximum thinning rate can be used to describe the forming limit of a simple sheet during incremental forming. During SPIF of the two kinds of materials, the forming limit angle

and the thinning rate of the sheet are decreased as the step size is increased. Since the maximum thinning rate obtained by the simulation is not much different from that obtained experimentally, the maximum thinning rate and the forming angle obtained from a simulation can be used in production.

As in Section 4.1.2, from the thinning rate zone and the angle zone of a forming limit diagram, we can obtain the maximum thinning rate and the maximum forming limit angle for a material by simulation. There is a non-safe zone above the forming limit curve, where cracking occurs. A part can be stably formed in the safe zone below the forming limit. The simulation method can quickly determine the maximum forming limit of 1060Al and 6061Al for different step sizes.
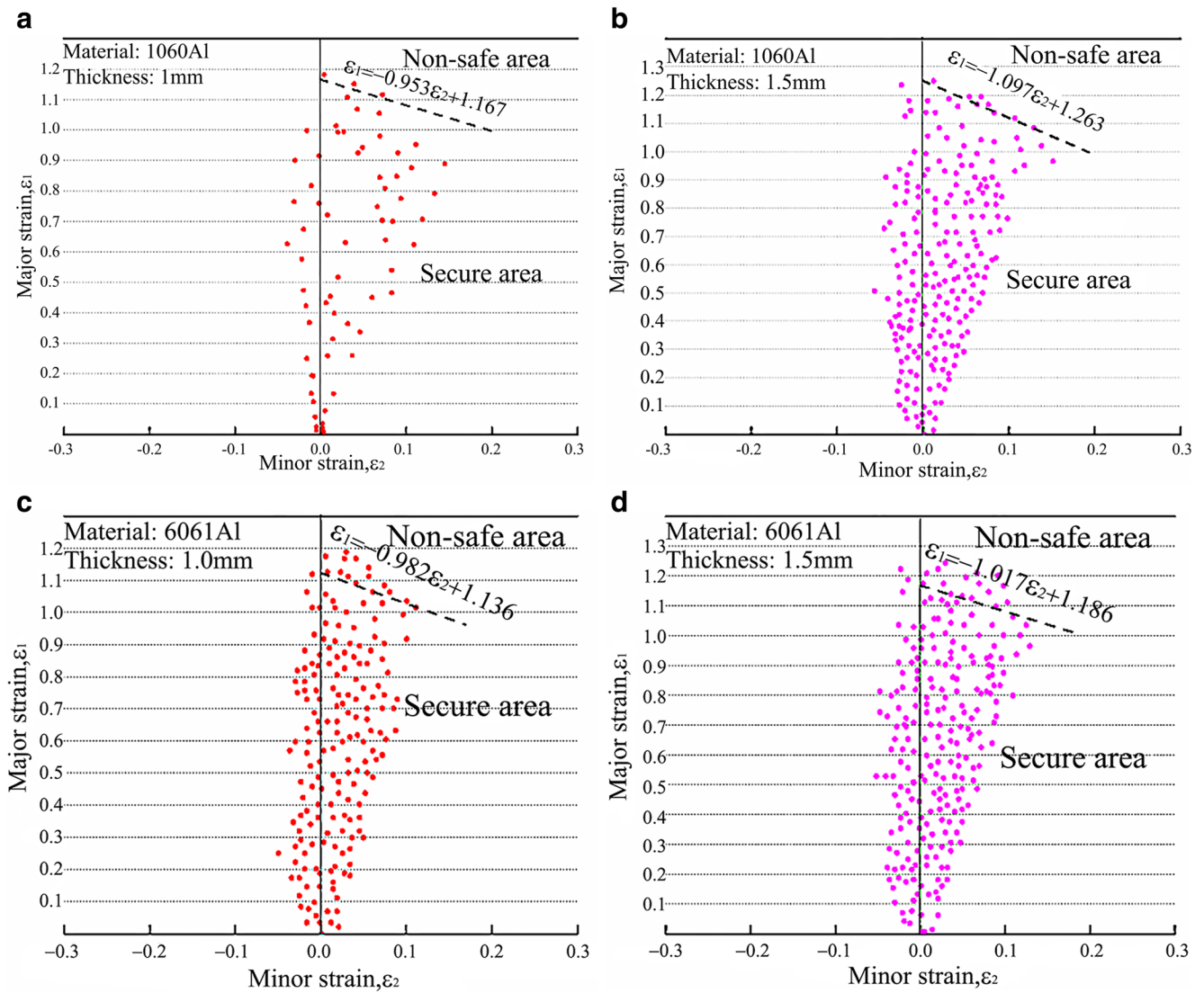
4.2.2 Effect of step size on the forming limit diagram

The ANSYS/LS-DYNA software was used to simulate SPIF of 1060Al and 6061Al plates at step sizes of 1.0 mm and 1.5 mm. Figure 18(a) and (b) show forming limit diagrams

Fig. 11 Simulated forming limit diagram: (**a**) 1060Al thickness = 1.0 mm, (**b**) 6061Al thickness = 1.0 mm
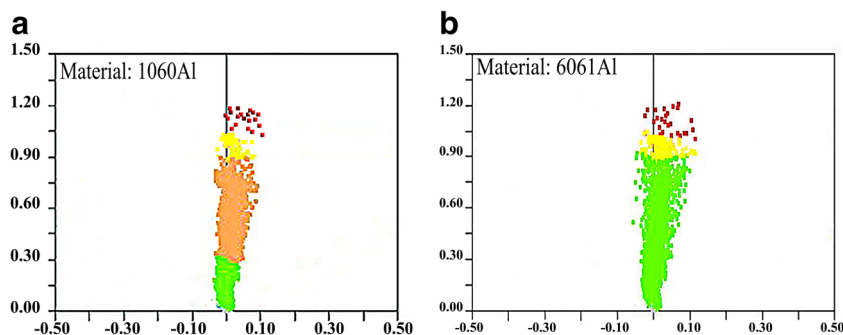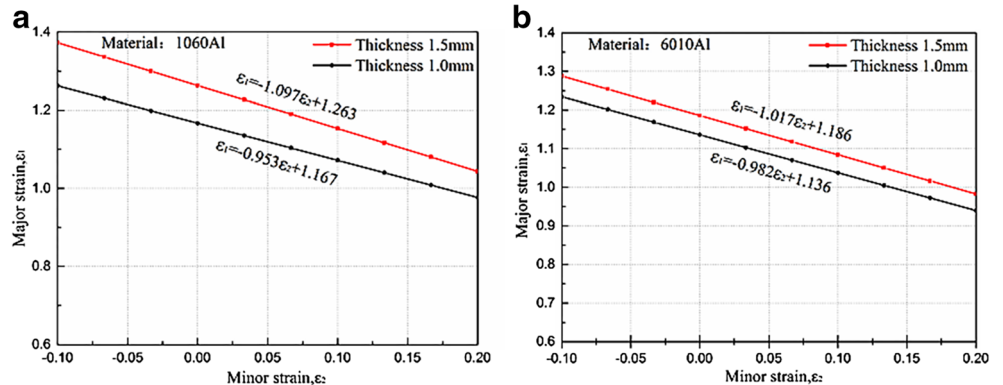
Fig. 12 Experimental forming limit diagrams: (**a**) 1060Al thickness = 1.0 mm, (**b**) 1060Al thickness = 1.5 mm, (**c**) 6061Al thickness = 1.0 mm, (**d**) 6061Al thickness = 1.5 mm

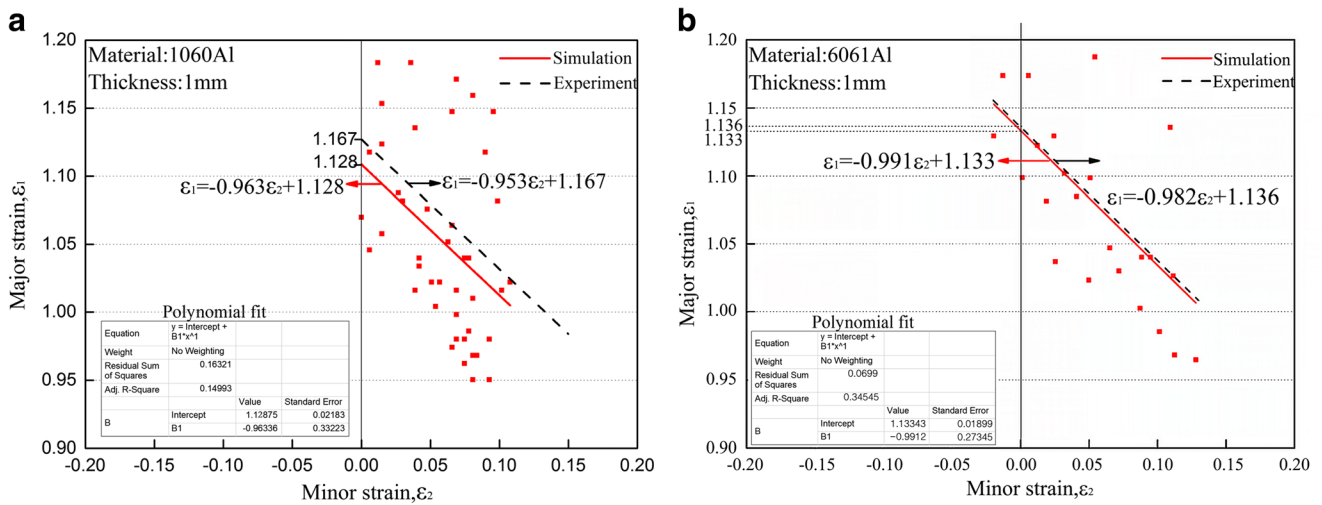Fig. 13 Forming limit of different initial sheet thickness of same material: (**a**) 1060Al, (**b**) 6061Al

Fig. 14 Comparison of forming limit lines between simulation and experiment: (**a**) 1060Al, (**b**) 6061Al

Table 5 Summary of thickness thinning rate for 1, 2, and 7 tests

Material	Step size (mm)	Forming limit angle (°)	Maximum thinning rate	
			Simulation	Experiment
1060Al	0.8	67.8	81.31%	84.95%
	1	67.4	79.38%	84.28%
	1.5	66.8	78.97%	83.01%
6061Al	0.8	67.2	79.14%	82.35%
	1	67.0	78.57%	81.58%
	1.5	66.2	77.64%	80.39%
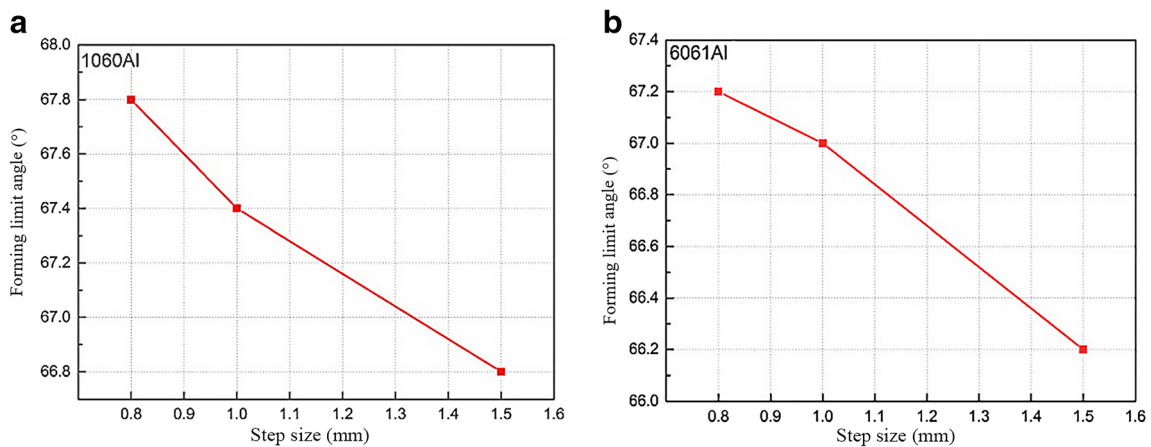
Fig. 15 Relationship between step size and forming limit angle: (**a**) 1060Al, (**b**) 6061Al
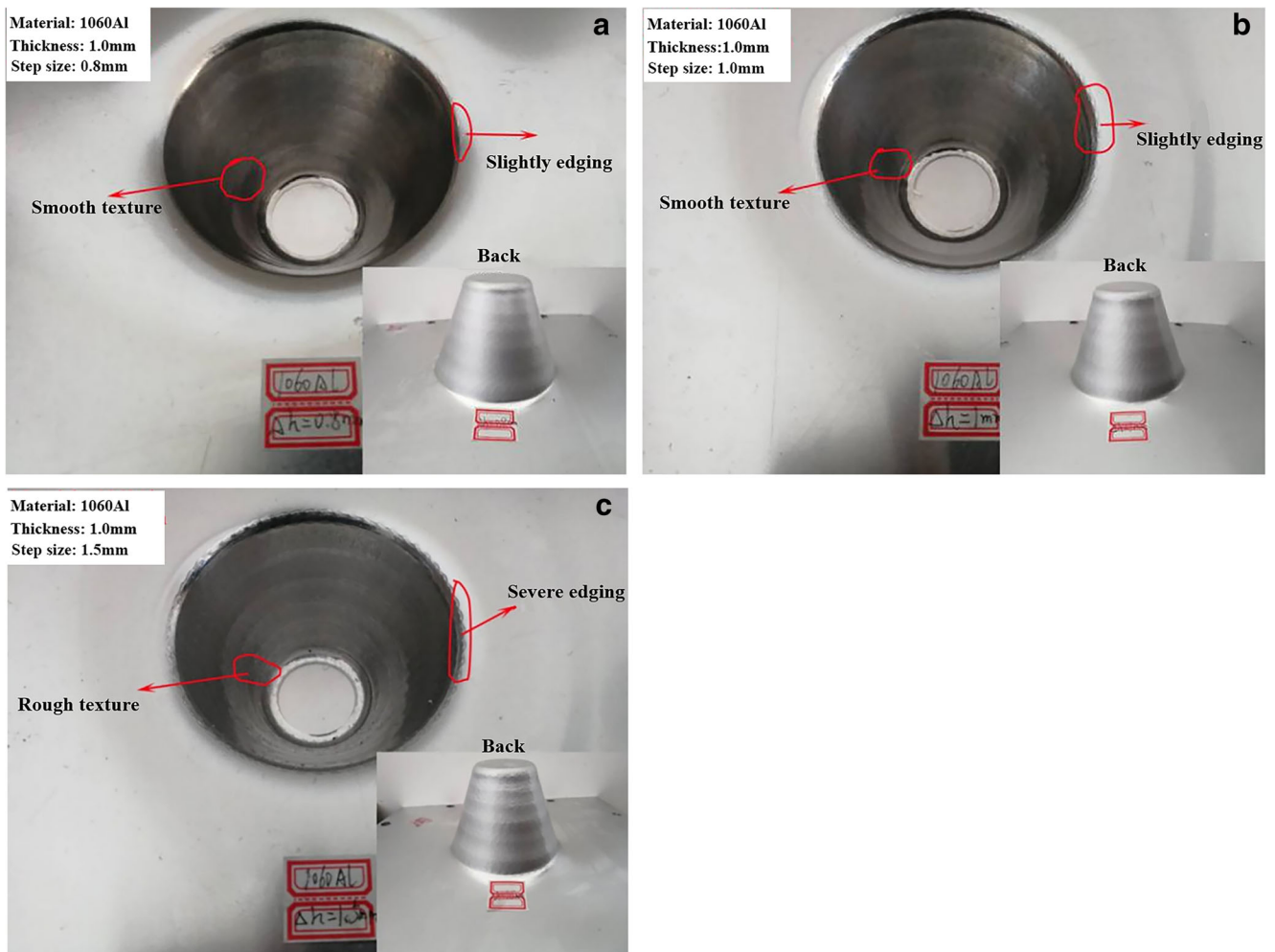
Fig. 16 Experimental part drawing with different step sizes: (**a**) step size = 0.8 mm, (**b**) step size = 1.0 mm, (**c**) step size = 1.5 mm
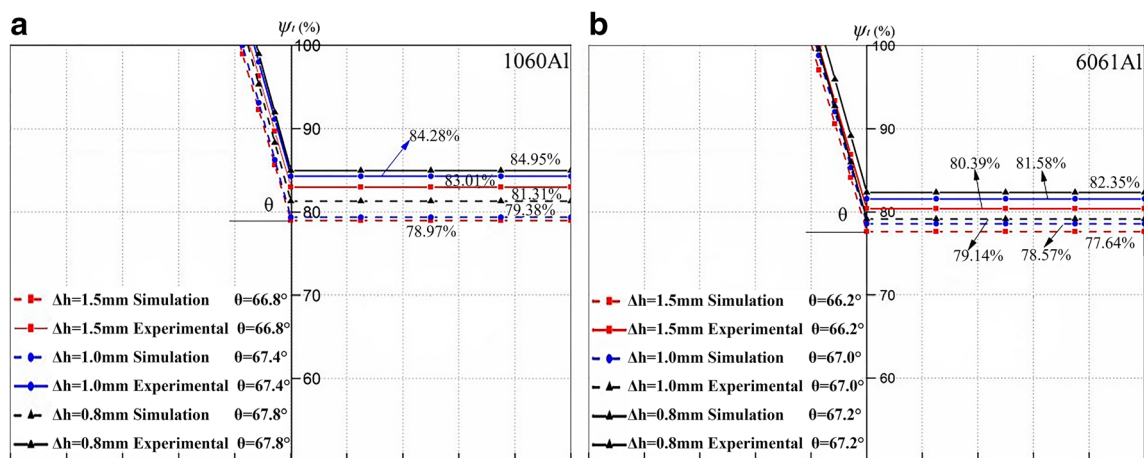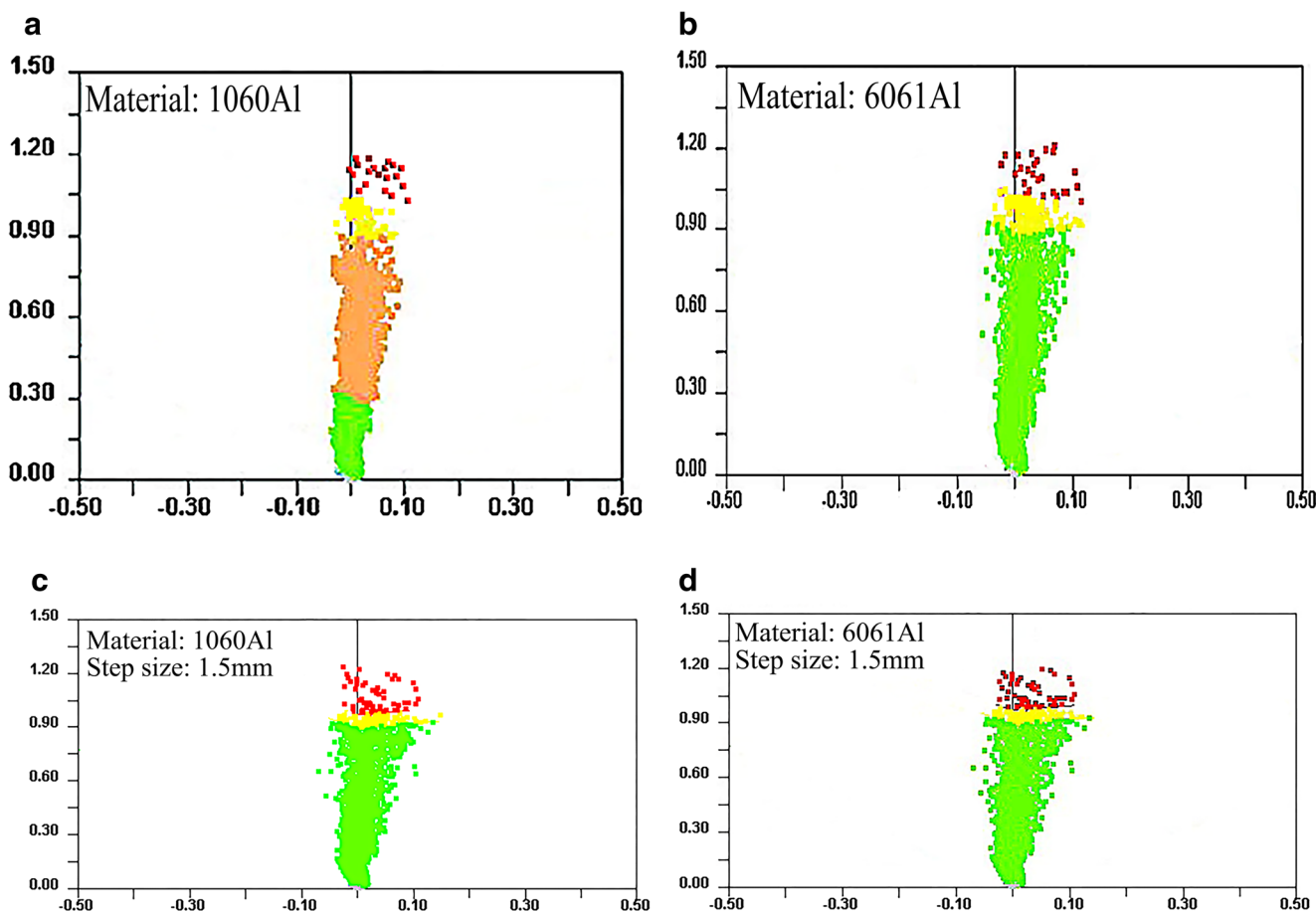

Fig. 17 Angle and thinning rate forming limit curves: (**a**) 1060Al, (**b**) 6061Al

Fig. 18 Simulation forming limit diagram: (**a**) 1060Al step size = 1.0 mm, (**b**) 6061Al step size = 1.0 mm, (**c**) 1060Al step size = 1.5 mm, (**d**) 6061Al step size = 1.5 mm

of 1060Al and 6061Al plates for SPIF with a step size of 1.0 mm. Figure 18(c) and (d) are simulated forming limit diagrams of 1060Al and 6061Al sheets for a step size of 1.5 mm.

Figure 19 shows experimental forming limit diagrams for 1060Al and 6061Al materials for different step sizes. The forming limit of the sheet is roughly a straight line with a slope of − 1, while the forming limit diagram in traditional sheet metal forming is a V-shaped line reported by Kim et al. [19].

It is convenient to judge whether the sheet is formed according to the straight line in the figure. The effect of different step sizes on the forming limit is shown in Fig. 20. The step size and the forming limit are inversely related.

We select the points in the red areas in Fig. 18 to create a scatter plot. In Fig. 21, we compare the numerical fitting line with the experimental fitting line. It can be seen that the experimentally obtained forming limit curve and the simulated forming limit curve have substantially the same slope; i.e., both are straight lines with a slope close to − 1.

In summary, both numerical simulations and experimental studies can be used to determine that the step size affects the

properties of a sheet during incremental forming. The lower the step size, the higher the forming limit of the sheet.

4.3 Effect of tool head radius on forming limit of SPIF sheet

In SPIF, the forming tool traverses the sheet layer by layer, causing metal flow and plastic deformation of the sheet until the target part is completed. The radius of the forming tool head affects the quality of the sheet. This section focuses on the effect of the radius of the forming tool head on the forming limit of a sheet during SPIF.

4.3.1 Effect of tool head radius on forming limit angle

From the SPIF experiments, the maximum forming angle and sheet thickness for different tool head radii were found. When the tool head has a radius of 4.0, 5.0, and 6.0 mm, other parameters are shown in Table 2. The results of limit angles are shown in Table 6. As the radius of the tool head increases, the limit angle increases. The limit angles are plotted in Fig. 22.
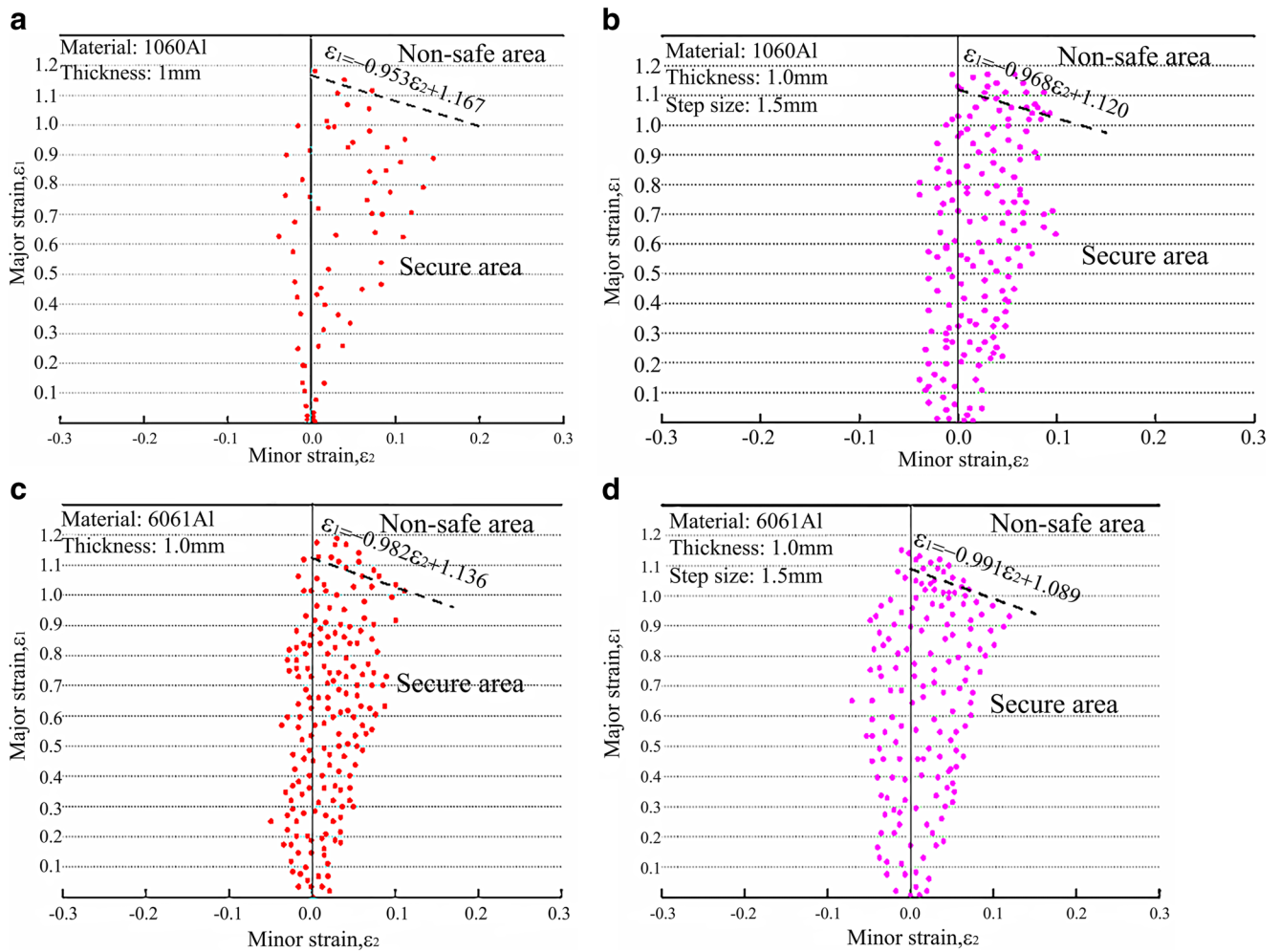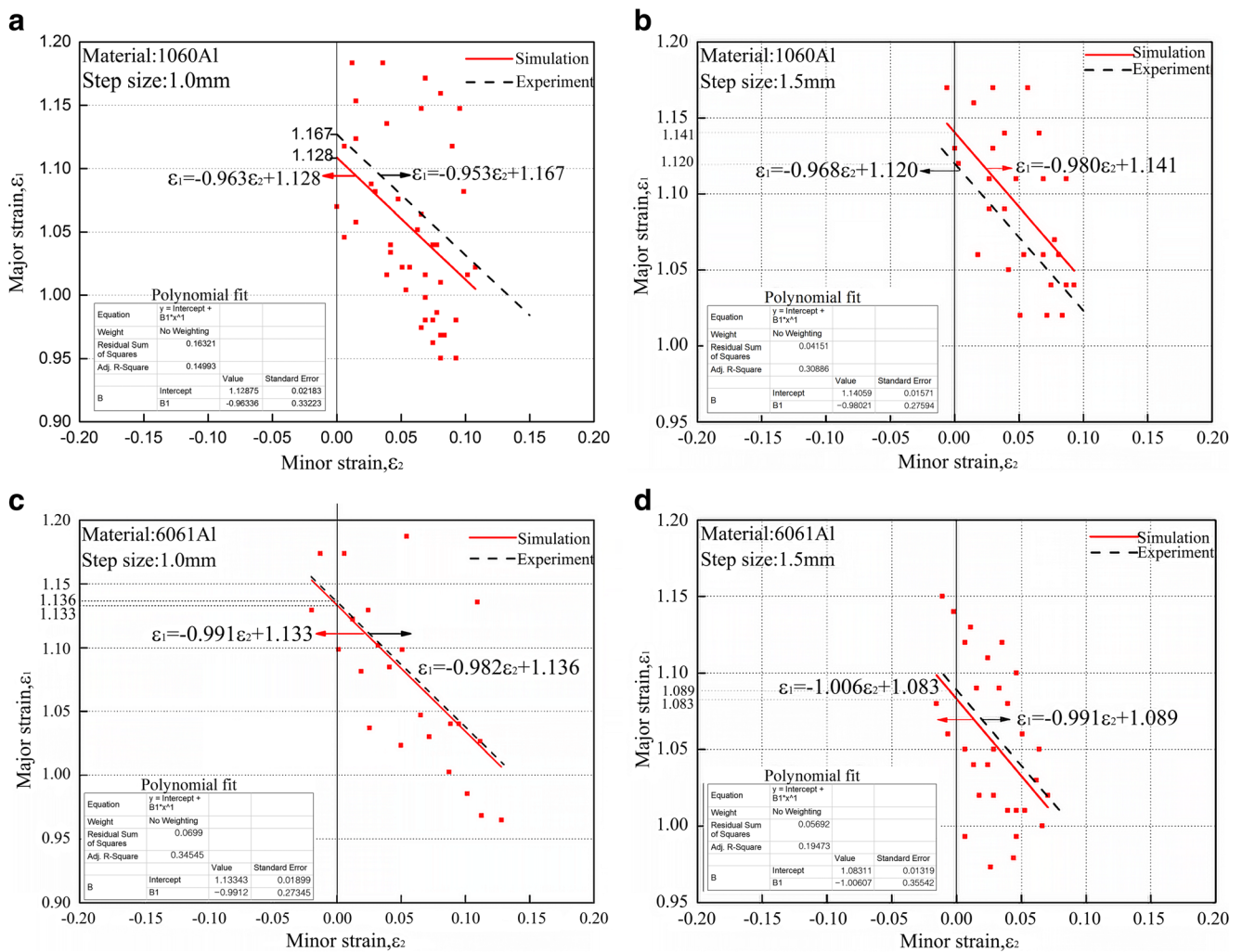
Fig. 19 Experimental forming limit diagram: (**a**) 1060Al step size = 1.0 mm, (**b**) 1060Al step size = 1.5 mm, (**c**) 6061Al step size = 1.0 mm, (**d**) 6061Al step size = 1.5 mm
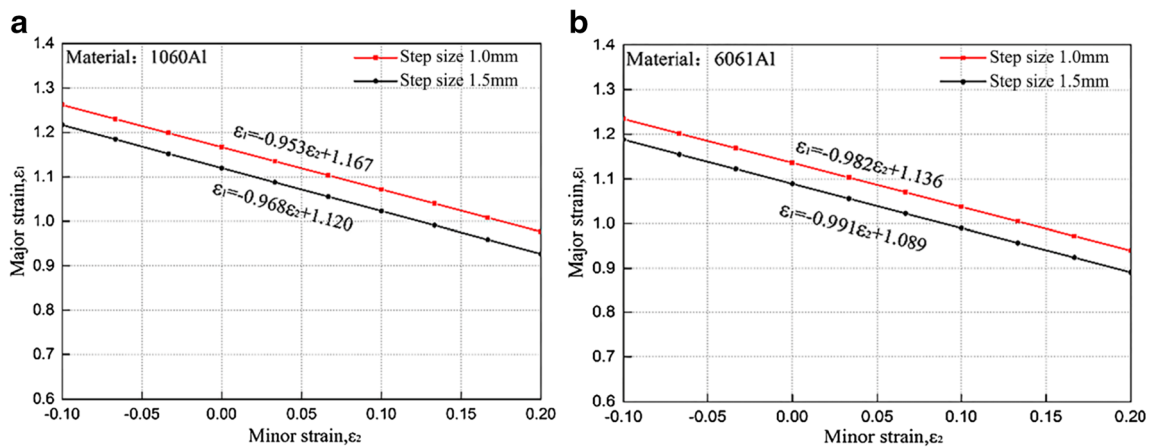
Fig. 20 Forming limit of different step sizes of same material: (**a**) 1060Al, (**b**) 6061Al

Fig. 21 Comparison of forming limit line between simulation and experiment: (**a**) 1060Al step size = 1.0 mm, (**b**) 1060Al step size = 1.5 mm, (**c**) 6061Al step size = 1.0 mm, (**d**) 6061Al step size = 1.5 mm

Table 6 Summary of thickness thinning rate for 1, 3, and 4 tests

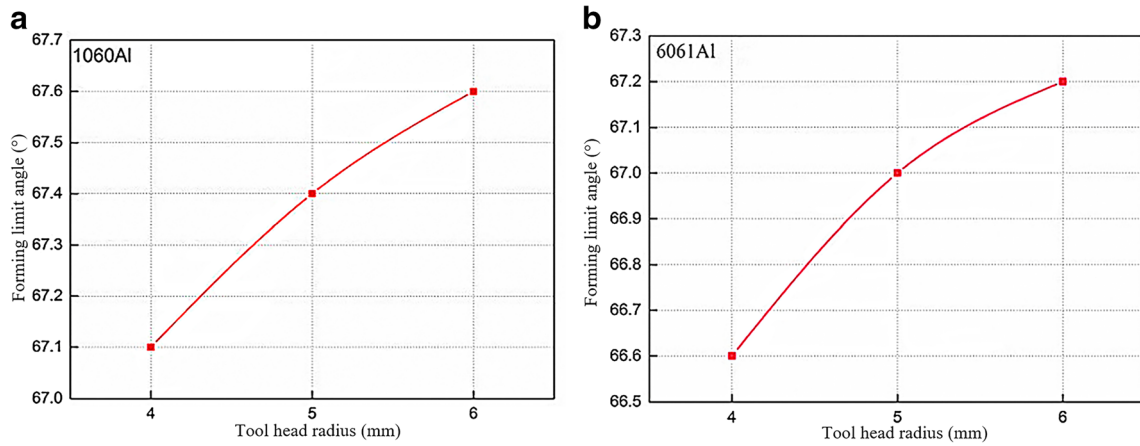| Material	Tool head radius	Forming limit angle	Maximum thinning rate	
	(mm)	(°)	Simulation	Experiment
1060Al	4	67.1	78.67%	82.59%
	5	67.4	79.38%	84.28%
	6	67.6	80.05%	84.92%
6061Al	4	66.6	77.21%	80.46%
	5	67.0	78.57%	81.58%
	6	67.2	79.53%	82.18%

Fig. 22 Relationship between tool head radius and forming limit angle: (**a**) 1060Al, (**b**) 6061Al
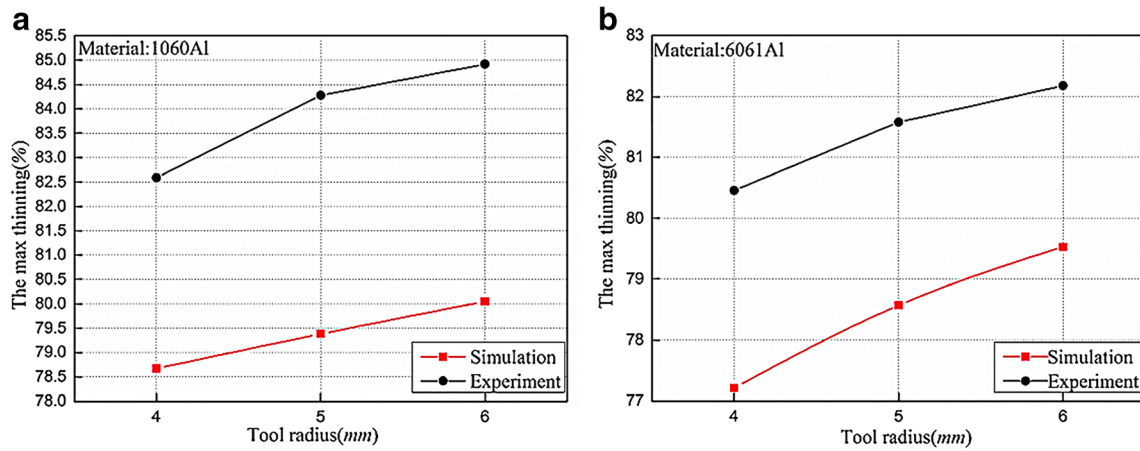

Fig. 23 Comparison of maximum thinning rate between different tool radius simulation and experiment: (**a**) 1060Al, (**b**) 6061Al
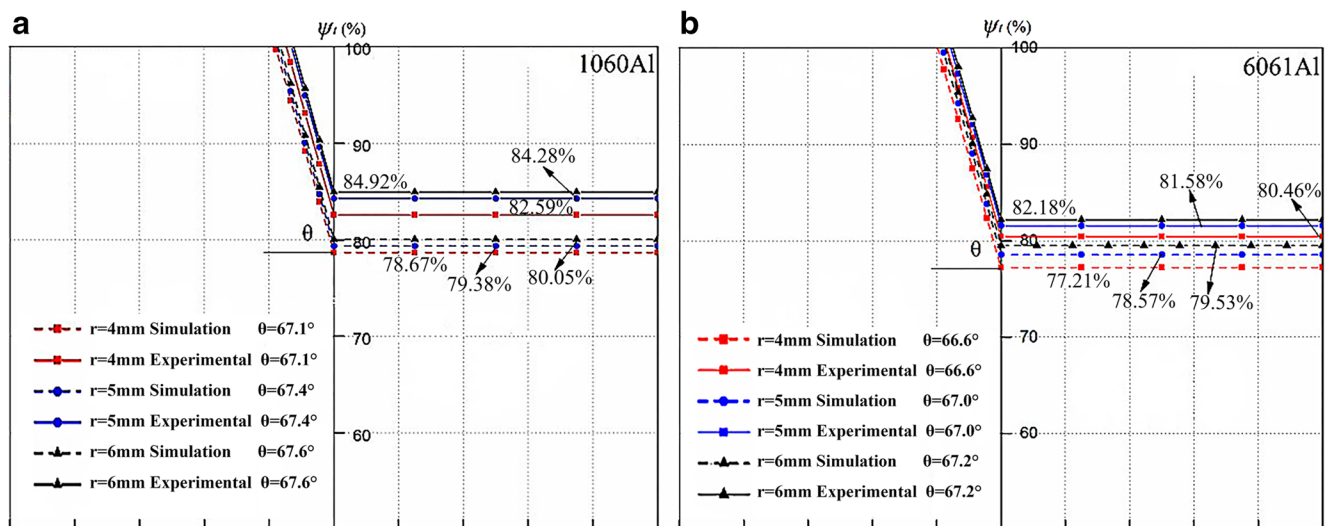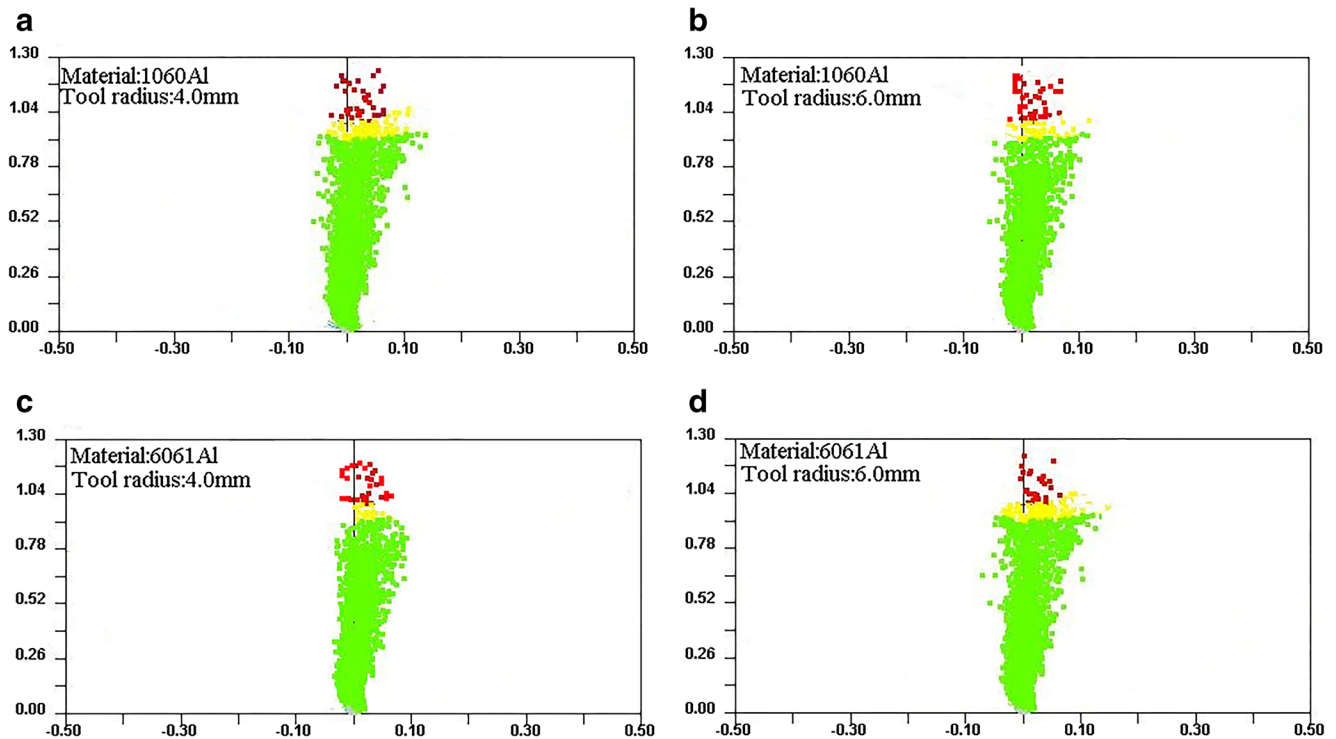

Fig. 24 Angle and thinning rate forming limit curves: (**a**) 1060Al, (**b**) 6061Al

Fig. 25 Simulation forming limit diagram: (**a**) 1060Al tool radius = 4.0 mm, (**b**) 1060Al tool radius = 6.0 mm, (**c**) 6061Al tool radius = 4.0 mm, (**d**) 6061Al tool radius = 6.0 mm

Figure 23 compares the maximum thinning rate obtained by simulation and that measured by the experiments. It can be seen from the figure that the slope of the maximum thinning rate for the simulations and the experiments is about the same and increases as the radius of the tool head increases.

Figure 24 shows the forming limit curves for the forming angle and the maximum thinning rate. It can be seen that the simulated forming limit region and the forming limit region obtained by experiment are not much different.

4.3.2 Effect of tool head radius on the forming limit diagram

Figure 18(a) and (b) are forming limit diagrams for a tool head radius of 5.0 mm. This section focuses on forming limit diagrams with tool head radii of 4.0 mm and 6.0 mm. Figure 25 shows the forming limit diagrams for the different tool head radii obtained by simulation.

Figure 26 shows experimental forming limit diagrams of the two materials drawn by the strain measurement grid method for different tool head radii. As can be seen from the figure, the slope of the forming limit for the sheet during incremental forming is a straight line of slope −1. The SPIF primary and secondary strain regions are, respectively, a safe zone and a non-

safe zone. We selected the highest point (red scatter) in the simulated limit diagrams in Fig. 25. We fitted lines to the values and compared them with the experimental fit lines. The results are shown in Fig. 27.

As shown in Fig. 27, the forming limit fits for a sheet machined by SPIF for different tool head radii obtained by experiment and simulation are very similar. The slopes of the straight lines are roughly −1. The experiments and simulations show that as the tool tip radius increases, the forming limits of the 1060Al and 6061Al sheets also increase.

5 Conclusions

In this paper, the forming limit of sheet metal during SPIF was studied with a numerical simulation and experimentally. The forming angle θ and maximum thinning rate ψ_t were used to describe the simple shape of a sheet in incremental forming. The forming limit in the process and the effects of the initial thickness, step size, and tool head radius on the forming limit of the sheet were analyzed. The main conclusions are as follows:

(1) The forming angle θ and the maximum thinning rate ψ_t can be used to describe the forming limit of a simple
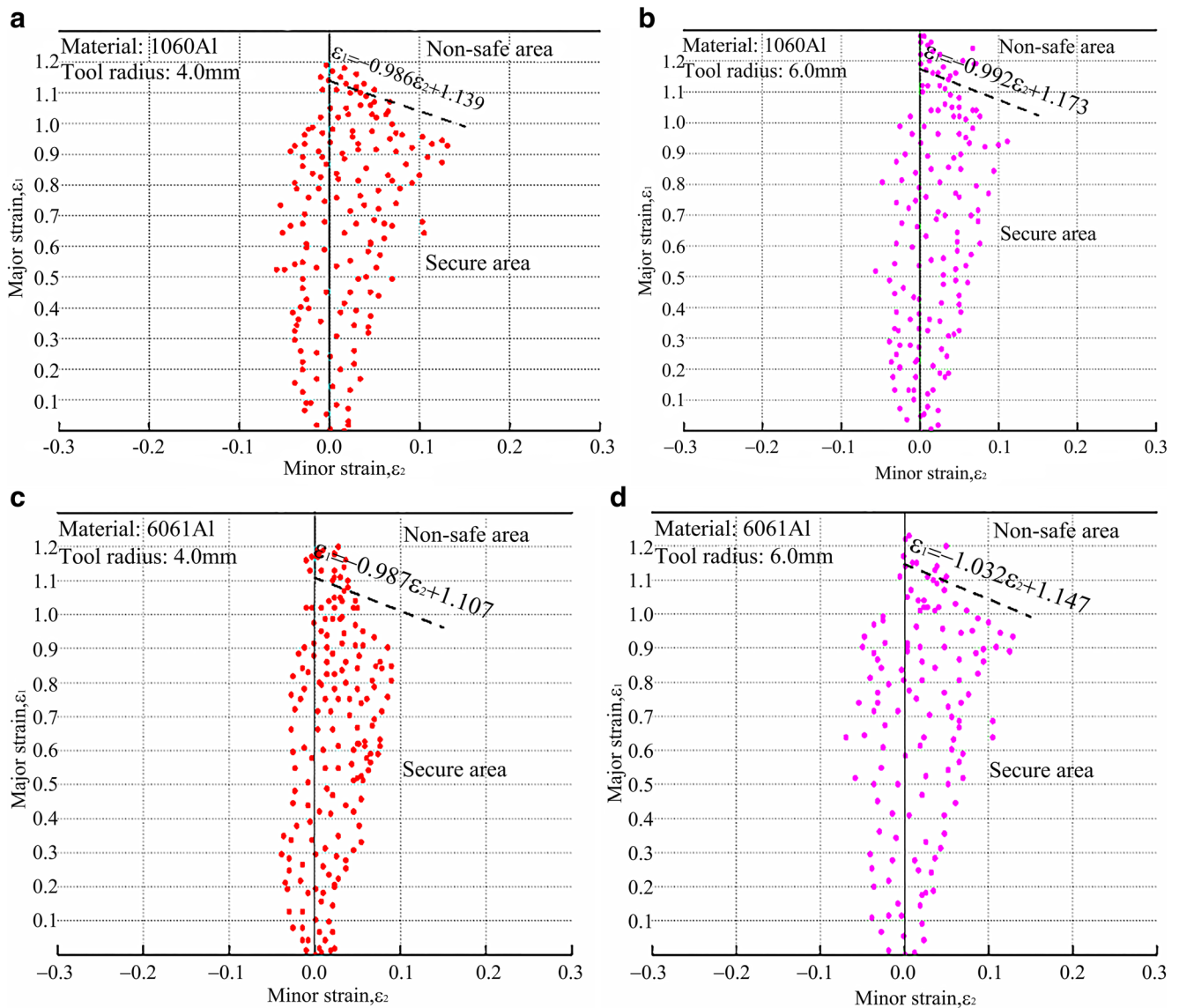
Fig. 26 Experimental forming limit diagram: (**a**) 1060Al tool head radius = 4.0 mm, (**b**) 1060Al tool head radius = 6.0 mm, (**c**) 6061Al tool head radius = 4.0 mm, (**d**) 6061Al tool head radius = 6.0 mm

shape sheet during incremental forming. The forming properties of a sheet during incremental forming can be analyzed more intuitively and conveniently. However, this method does not apply to the forming limit for asymmetrical or complex forming, or for a variable forming angle.

(2) Through the numerical simulations and experiments, we obtained forming limit diagrams of sheet metal during SPIF. We fitted a forming limit curve, which is a straight line with a slope of roughly − 1.

(3) The forming limit of a sheet during incremental forming depends on the initial thickness. As the initial sheet thickness increases, the forming limit of the sheet improves significantly.

(4) The forming limit of a sheet during incremental forming also depends on the step size. As the step size decreases, the sheet forming limit improves significantly.

(5) The forming limit of a sheet during incremental forming further depends on the radius of the tool head. As the radius increases, the forming limit of the sheet increases.
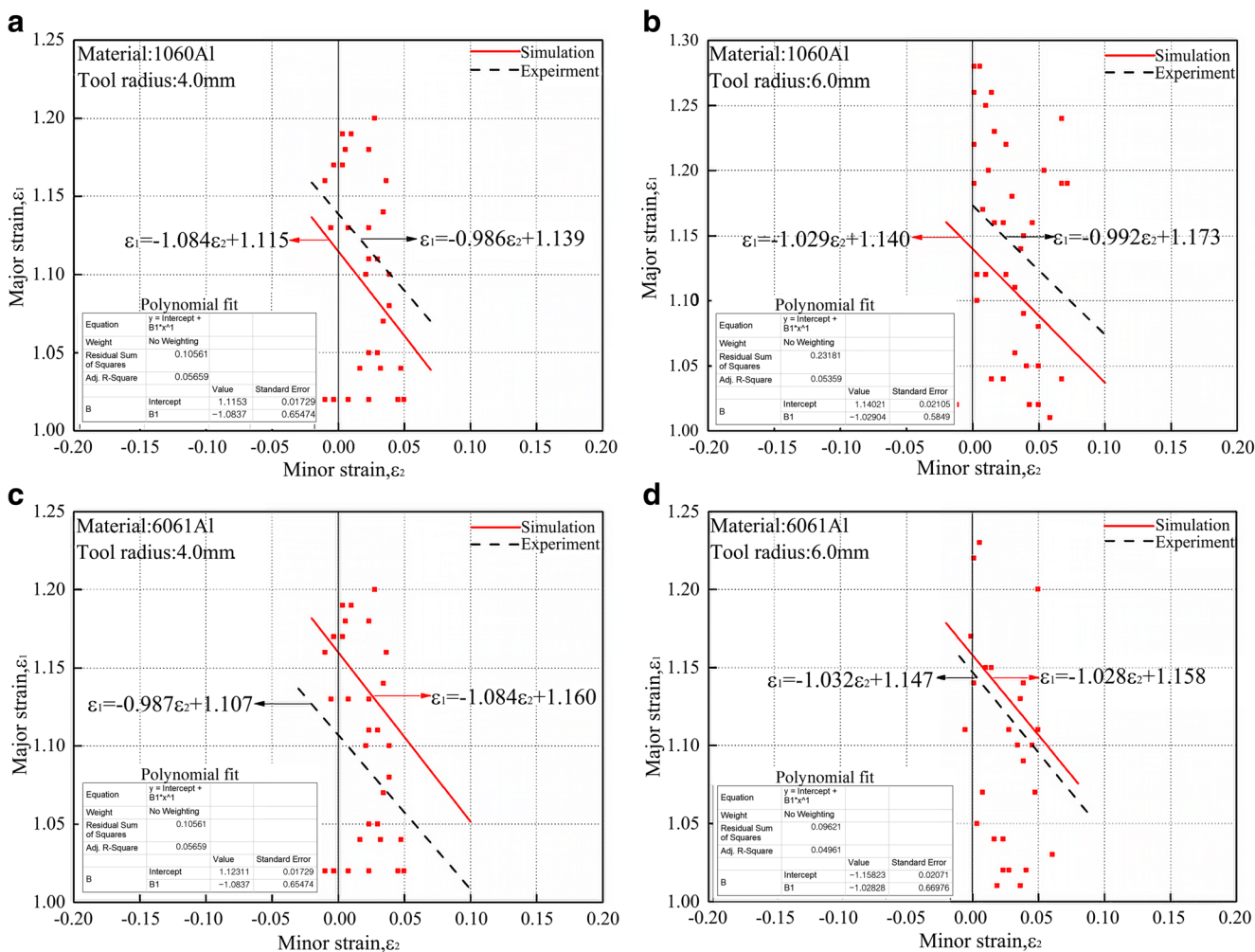
Fig. 27 Comparison of forming limit line between simulation and experiment: (**a**) 1060Al tool head radius = 4.0 mm, (**b**) 1060Al tool head radius = 6.0 mm, (**c**) 6061Al tool head radius = 4.0 mm, (**d**) 6061Al tool head radius = 6.0 mm

Compliance with ethical standards

Ethical approval   Not applicable.

Consent to participate   Not applicable.

Consent to publish   Not applicable.

Competing interests   The authors declare that they have no competing interests.

References

1. Gu J, Sol H, He SX, Bael AV, Albert, Duflou J (2007) Full field optical measurement of large deformation fields in single point incremental forming (SPIF) Processes. The Abstracts of ATEM : International Conference on Advanced Technology in Experimental Mechanics : Asian Conference on Experimental Mechanics. 2007.6. _OS9–1. https://doi.org/10.1299/jsmeatem.2007.6._OS9-1-1-1

2. Nguyen TH, Le KD, Nguyen NP, Nguyen HB, Nguyen TN, Vo T (2017) The effect of heating to the formability of titanium sheet by SPIF Technology. Key Eng Mater 749:171–177. https://doi.org/10.4028/www.scientific.net/KEM.749.171

3. Centeno G, Morales-Palma D, Gonzalez-Perez-Somarriba B, Bagudanch I, Egea-Guerrero JJ, Gonzalez-Perez LM, García-Romeu ML, Vallellano C (2017) A functional methodology on the manufacturing of customized polymeric cranial prostheses from CAT using SPIF. Rapid Prototyp J 23(4):771–780. https://doi.org/10.1108/RPJ-02-2016-0031

4. McAnulty T, Jeswiet J, Doolan M (2017) Formability in single point incremental forming: a comparative analysis of the state of

the art. CIRP J Manuf Sci Technol 16:43–54. https://doi.org/10.1016/j.cirpj.2016.07.003

5. Uheida EH, Oosthuizen GA, Dimitrov DM, Bezuidenhout MB, Hugo PA (2018) Effects of the relative tool rotation direction on formability during the incremental forming of titanium sheets. Int J Adv Manuf Technol 96:3311–3319. https://doi.org/10.1007/s00170-018-1837-9

6. Raju C, Sathiya Narayanan C (2016) FLD and fractography analysis of multiple sheet single point incremental forming. Trans Indian Inst Metals 69(6):1237–1243. https://doi.org/10.1007/s12666-015-0679-5

7. Eyckens P, Bael AV, Houtte PV (2009) Marciniak–Kuczynski type modelling of the effect of through-thickness shear on the forming limits of sheet metal. Int J Plast 25(12):2249–2268. https://doi.org/10.1016/j.ijplas.2009.02.002

8. Buffa G, Campanella D, Fratini L (2013) On the improvement of material formability in SPIF operation through tool stirring action. Int J Adv Manuf Technol 66:1343–1351. https://doi.org/10.1007/s00170-012-4412-9

9. Ramkumar K, Baskar N, Elangovan K, Sathiya Narayanan C, Selvarajan KA, Jesuthanam CP (2020) Comparison of multi point incremental forming tool with single point incremental forming tool using FLD, fractography and 3D-surface roughness analysis on Cr/Mn/Ni/Si based stainless steel. Silicon. https://doi.org/10.1007/s12633-020-00468-4

10. Mirnia MJ, Shamsari M (2017) Numerical prediction of failure in single point incremental forming using a phenomenological ductile fracture criterion. J Mater Process Technol 244:17–43. https://doi.org/10.1016/j.jmatprotec.2017.01.029

11. Zhan XP, Wang ZH, Li M, Hu Q, Chen J (2020) Investigations on failure-to-fracture mechanism and prediction of forming limit for aluminum alloy incremental forming process. J Mater Process Technol 282:116687. https://doi.org/10.1016/j.jmatprotec.2020.116687

12. Zhang FF, He K, Dang XB, Du RX (2018) Experimental and numerical study on one flexible incremental bending process. Int J Adv Manuf Technol 96:2643–2655. https://doi.org/10.1007/s00170-018-1777-4

13. Esmaeilpour R, Kim H, Park T, Pourboghrat F, Mohammed B (2017) Comparison of 3D yield functions for finite element simulation of single point incremental forming (SPIF) of aluminum 7075. Int J Mech Sci 133:544–554. https://doi.org/10.1016/j.ijmecsci.2017.09.019

14. Silva AV, Postal C, 5156 (San Paulo, BR) (1972) Control system for tandem rolling mill based on the constant volume principle. United States Patent 3688532. https://www.freepatentsonline.com/3688532.html. Accessed 24 Feb 2019

15. Cho CH, Shin HS, Chu CN (2014) Micropatterning on cylindrical surfaces via electrochemical etching using laser masking. Appl Surf Sci 301:442–450. https://doi.org/10.1016/j.apsusc.2014.02.095

16. Nichols JJ, Mitchell GL, King-Smith PE (2005) Thinning rate of the precorneal and prelens tear films. Invest Ophthalmol Vis Sci 46(7):2353–2361. https://doi.org/10.1167/iovs.05-0094

17. Lee WJ, Kim YK, Park KH, Jeoung JW (2017) Trend-based analysis of ganglion cell–inner plexiform layer thickness changes on optical coherence tomography in glaucoma progression. Ophthalmology 124(9):1383–1391. https://doi.org/10.1016/j.ophtha.2017.03.013

18. Kim JG, Park IJ (2015) Aluminum alloy composition, aluminum extrusion tube and fin material with improved corrosion durability comprising same, and heat exchanger constructed of same. WO/2015/046940. https://www.freepatentsonline.com/WO2015046940.html. Accessed 2 March 2019

19. Kim JH, Ko DH, Ko DC, Kim BM (2016) Forming limit diagrams of tailor rolled blank in hot stamping and its verification. Adv Mater Process Technol 2(4):409–417. https://doi.org/10.1080/2374068X.2016.1147811

Publisher's note Springer Nature remains neutral with regard to jurisdictional claims in published maps and institutional affiliations.